

2-Dimensional beamsteering using dispersive deflectors and wavelength tuning

Trevor Chan,^{1,*} Evgeny Myslivets,¹ and Joseph E. Ford,¹

¹*Department of Electrical and Computer Engineering, University of California, San Diego, 9500 Gilman Dr. La Jolla, CA 92093, USA*

*Corresponding author: tkc@ucsd.edu

Abstract: We introduce a 2D beams scanner which is controlled by wavelength tuning. Two passive dispersive devices are aligned orthogonally to deflect the optical beam in two dimensions. We provide a proof of principle demonstration by combining an arrayed waveguide grating with a free space optical grating and using various input sources to characterize the beams scanner. This achieved a discrete 10.3° by 11° output field of view with attainable angles existing on an 8 by 6 grid of directions. The entire range was reached by scanning over a 40 nm wavelength range. We also analyze an improved system combining a virtually imaged phased array with a diffraction grating. This device is much more compact and produces a continuous output scan in one direction while being discrete in the other.

©2008 Optical Society of America

OCIS codes: (060.2605) Free-space optical communications; (050.1970) Diffractive optics; (080.1238) Array waveguide devices.

References and links

1. G. Nykola, G. Raybon, B. Mikkelsen, B. Brown, P. F. Szajowski, J. J. Auburn and H. M. Presby, "A 160 Gb/s free space transmission link" in *Proceedings of Conference on Lasers and Electro-optics*, (Washington, D.C., 2000), pp. 687-688.
2. M. Cole and K. Kiasaleh, "Signal intensity estimators for free-space optical communications through turbulent atmosphere." *IEEE Photon. Technol. Lett.* **16**, 2395-2397, (2004).
3. L. Zhou, J. M. Kahn, K. S. J. Pister, "Scanning micromirrors fabricated by an SOI/SOI wafer-bonding process," *J. Microelectromech. Syst.* **15**, 24-32, (2006).
4. V. Nikulin, R. Khandekar, J. Sofka, "Performance of a laser communication system with acousto-optic tracking: An experimental study," *Proc. SPIE* **6105**, 61050C, (2006).
5. A. Yariv, P. Yeh, *Optical Waves in Crystals*, (Wiley, Hoboken, 2003), Chap. 8.
6. B. Winker, M. Mahajan, M. Hunwardsen, "Liquid crystal beam directors for airborne free-space optical communications," in *2004 IEEE Aerospace Conference Proceedings*, (Big Sky, Montana, March 2004).
7. I. Filinski and T. Skettrup, "Fast dispersive beam deflectors and modulators," *IEEE J. Quantum Electron.* **18**, 1059-1062, (1982).
8. T. K. Chan, J. Karp, R. Jiang, N. Alic, S. Radik, C. F. Marki, J. E. Ford, "1092 channel 2-D array demultiplexer for ultralarge data bandwidth," *J. Lightwave Technol.* **25**, 719-725, (2007).
9. J. E. Simsarian, A. Bhardwaj, J. Gripp, K. Sherman, Y. Su, C. Webb, L. Zhang, M. Zirngibl, "Fast switching characteristics of a widely tunable laser transmitter," *IEEE Photon. Technol. Lett.* **15**, 1038-1040, (2003).
10. M. Shirasaki, "Virtually imaged phased array," *Fujitsu Sci. Tech. J.* **35**, 113-125, (1999).

1. Introduction

Free-space optical (FSO) communications provide a communication link by encoding information in a laser beam between the points of communication. A FSO communication link is sometimes chosen over RF wireless communications because the nature of the laser allows secure, high-bandwidth wireless links. However, an additional complexity in establishing a communication link is that the optical beam must be aimed to its targeted receiver. This is routinely accomplished between stationary nodes¹ where large angle, active alignment is not required.

This method becomes more complex when the points of communication (either or both) become mobile, as this requires real-time alignment. In order to maintain the communication link, the laser beam must be constantly pointed at the receiver, thereby requiring fast beamsteering speeds for a large angular range. In addition to the relative motion of the receiver, atmospheric effects such as scintillation may also misdirect the beam, thereby calling for beamsteering speeds much less than the pointing errors caused by scintillation (on order of a few milliseconds²).

Several methods have been used to steer a beam over a range of angles. An obvious solution involves simply reflecting the light off a tiltable mirror, such as a galvanometric scanner. Although these large mirrors suffer in speed and power dissipation, tiltable mirrors can be small when they are made as microelectromechanical systems³ (MEMS). These mirrors operate considerably faster with multi-kHz sweeping speeds, but are limited to aperture sizes of a few millimeters. This trade-off between size and speed is a concern because a smaller aperture leads to a greater beam divergence which in turn decreases the range. Acousto-optic⁴ deflectors are limited in their total angular range and electro-optic⁵ crystals require kilovolt drive voltages to obtain an adequate angular range and aperture.

The ideal beamsteering device for FSO links would have a combination of fast switching speeds, large aperture, pointing accuracy and low power. Usually, the desired performance parameters are intertwined such that when high speed (> kHz) is achievable, it is reached at the expense of one of the other parameters.

An indirect way to increase aperture size without decreasing performance is by segmenting the aperture into an array of sub-apertures. Each sub-aperture functions as its own device and therefore, maintains the advantages of a small aperture device. However, the cost of segregation is that each aperture has to be phase matched to one another.

Alternatively, phase matching itself can be used as a means of beamsteering. This has been done with arrays of liquid crystals⁶ where the phase delay from each element in an array is given a phase delay such that emitting wavefronts match in the desired beam propagation direction. However, liquid crystals can only be tuned at kilohertz speeds.

In our work, we accomplish phased array beamsteering with passive phased arrays instead of active ones. Passive phased arrays can be diffraction gratings, arrayed waveguide gratings (AWG) or virtually imaged phased arrays (VIPA). More conventional 'beamsteering' optics control the properties of the steering device to deflect an entire wavefront (or image). Instead, orthogonal diffraction uses fixed-response optics and directs a single beam of monochromatic light by changing the wavelength of the beam. This effectively decouples the speed dependence from the other parameters by utilizing wavelength flexibility as another degree of freedom; one that can have a negligible effect on the FSO link.

2. 2-D Wavelength beam-scanning concept

A diffraction grating has the ability to disperse light in one dimension. When a single wavelength is transmitted through a grating, it is diffracting according to the grating equation, Eq. (1), where P is the grating period, m the diffraction order, λ the wavelength, and θ_m and θ_i the transmitted and incident angles respectively.

$$P(\sin \theta_m - \sin \theta_i) = m\lambda \quad (1)$$

This equation shows that the deflection by the grating changes as the wavelength is changed. Thus, when a laser is tuned across a wavelength range, the beam scans along a line⁷. This alone is insufficient for FSO pointing and tracking since objects exist in a 2-dimensional field of view. To reach the second dimension, we can include another diffraction grating that is oriented orthogonally to the first. This arrangement is shown in Fig. 1.

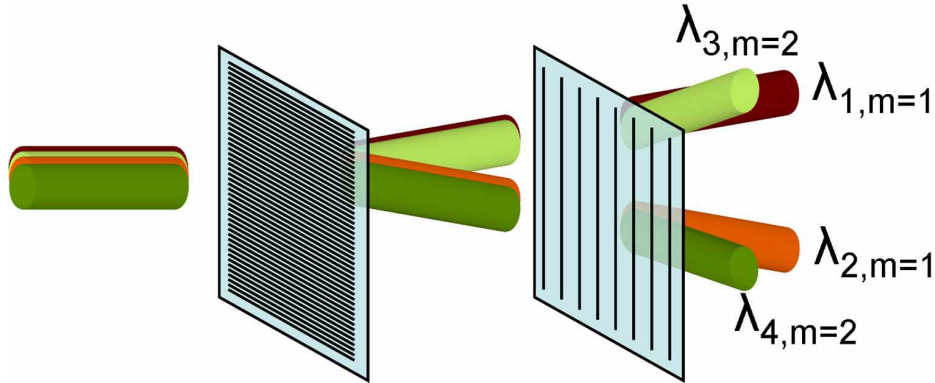


Fig. 1. 2 diffraction gratings oriented to achieve beams scanning in 2 dimensions. The difference in diffraction orders between the two diffractive structures allows for raster scanning as the wavelength is increased.

There are three characteristics which these gratings must have in order to function as a viable beam scanner that raster scans an entire 2-dimensional range. Firstly, both gratings should be fabricated such that most of the power is diffracted into one diffraction order. For example, in the case of a diffraction grating, a blaze angle would be required to restrict the power within an angular range that contains only one order. Second, the free spectral range of the lower order grating should be greater than the total wavelength scanning range. Thirdly, the total wavelength range should be greater than N times the free spectral range of the higher order grating, where N is the number of lines that are scanned across in the raster scan. When the second and third conditions are combined, a scan through the wavelength range will make one pass across the angular range of one grating while also making N passes through the range of the other. Since the gratings are oriented orthogonally, this creates a raster scan through a 2-D range of angles.

2.1 An AWG and a free space optical grating

One such arrangement that can meet the above criteria is an AWG followed by a free-space optical grating. The AWG has high dispersion because it operates in a high diffraction order. The diffraction order is determined by the increment in length, ΔL , between adjacent waveguides in the array, as defined by Eq. (2). Here, n_{awg} is the index of refraction of the waveguides and λ_m is the central output wavelength within the m^{th} diffraction order.

$$m = \frac{n_{\text{awg}} \Delta L}{\lambda_m} \quad (2)$$

The wavelength separation between diffraction orders is known as the free-spectral range (FSR). Equation (3) gives the FSR which is directly related to the final angular separation created by the diffraction grating.

$$FSR = \lambda_m - \lambda_{m+1} = \frac{\lambda_m}{m+1} \quad (3)$$

To determine all of the achievable directions, we must first know the exact wavelengths that are transmitted through our system. When we assume no wavelength dependant losses from reflections and transmission through optical materials, the transmitted wavelengths from our system are entirely determined by the diffractive properties of the AWG. To explore this, we start with the grating equation, and modify it to account for optical path delays in the AWG.

This yields Eq. (4) which now includes the index of the waveguides, n_{avg} , and the phase shift induced by the incremental length, ΔL , of successive waveguides.

$$n_{avg} P_{avg} (\sin \theta_m - \sin \theta_i) + n_{avg} \Delta L = m \lambda_m \quad (4)$$

In the AWG, the diffracted light out of the waveguide array is coupled into another array of output waveguides. Each of these waveguide channels collect the light at a certain angle, θ_N , coming out of the waveguide array. The wavelength at channel N and order m is found by isolating λ_m in Eq. (4) to arrive at Eq. (5).

$$\lambda_m = \frac{n_{avg}}{m} (\Delta L - P_{avg} \sin \theta_i) + \frac{n_{avg} P_{avg}}{m} \sin \theta_m \quad (5)$$

Here, we make the assumption that the output waveguides are arranged with an angular period θ_o , and that the output waveguides are centered such that θ_m is zero at the middle of the output array. When these are assumed, the first term on the right hand side of Eq. (5) is equal to the wavelength hitting the middle of the array, λ_c . These are found using Eq. (3). With these considerations, we now arrive at Eq. (6) where N is the output channel number and N_{max} is the total number of channels.

$$\lambda_{N,m} = \lambda_c + \frac{n_{avg} P_{avg}}{m} \sin \left[\theta_o \left(N - \frac{N_{max} + 1}{2} \right) \right] \quad (6)$$

Eq. (6) can be rewritten as Eq. (7) to explicitly yield N .

$$N = \frac{\sin^{-1} \left[\frac{m(\lambda_{N,m} - \lambda_c)}{n_{avg} P_{avg}} \right]}{\theta_o} + \frac{N_{max} + 1}{2} \quad (7)$$

The wavelengths within a diffraction order are separated spatially into free-space by the V-groove array. The output array of spots yielded by the v-groove array (pitch P_v) is re-imaged by the free-space grating demultiplexer before it is directed by the output lens (with f_o focal length). The output angle is given by Eq. (8).

$$\tan \theta_1 = \frac{P_v \left(N - \frac{N_{max} + 1}{2} \right)}{f_o} \quad (8)$$

The output angle in the orthogonal direction is created by the dispersion of the diffraction orders by the free-space grating demultiplexer. This demultiplexer might contain a 4-f imaging system with a reflection grating of period P_g , tilted by θ_g , at the Fourier plane and uses identical Fourier lenses with focal length f . The resulting output angle deflection caused by the diffraction grating is given by Eq. (9).

$$\tan \theta_2 = \frac{f}{f_o} \tan \left[\sin^{-1} \left(\frac{m \lambda}{P_g} + \sin \theta_g \right) + \theta_g \right] \quad (9)$$

3. Experimental setup

For our experimental demonstration of beamscanning, we used the system illustrated in Figs. 2 and 3. We used a JDSU 1x8 channel arrayed waveguide grating as the first diffractive element which operated in the 194th diffraction order at 1550 nm. Since the AWG gives discrete outputs at specific wavelengths, the achievable scanning angles exist in a nearly rectangular array rather than a set of lines. The AWG channels were transferred into free space through a 635 μm pitch v-groove array. This led into a free space optical grating demultiplexer, taken from a Network Photonics WDM switch, consisting of a 100 mm focal length Fourier lens followed by a 3rd order, 300 lp/mm reflection grating (Newport catalog code 53-^{*}013R). The architecture is similar to that used in our prior work in developing a large channel wavelength demultiplexer⁸. Like the demultiplexer, the output from the two demultiplexers is a grid of single mode Gaussian spots where each one corresponds to a different wavelength. This is converted into a beam scanner with the addition of a gold mirror (to divert the light away from the components) and a Nacet Vision 8x, 25 mm focal length microscope objective to collimate and direct the beam.

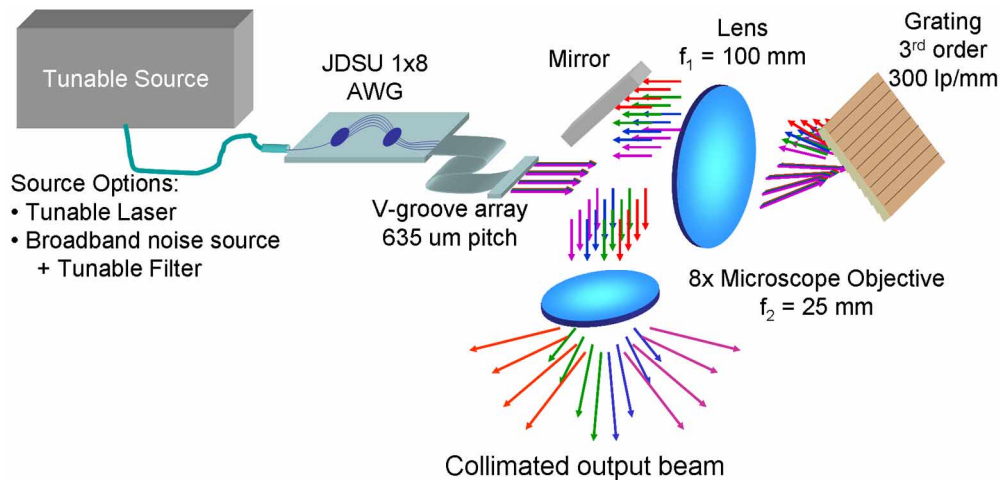


Fig. 2. System and components used to demonstrate beamscanning. The demultiplexed channels from the AWG are ejected into free space by a V-groove array which sits at the focal plane of a Fourier lens. This lens is part of a free space grating demultiplexer which separates the multiple orders from the AWG. The output is focused at the focal plane of a microscope objective which collimates and directs the light.

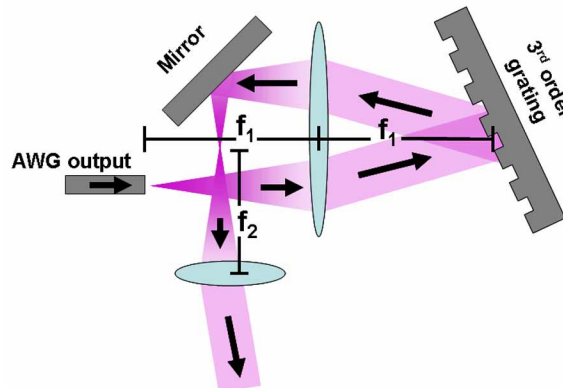


Fig. 3. 2-dimensional illustration of a monochromatic beam propagating through the system.

The AWG and free-space optical grating were both designed for the C-band (1530 – 1562 nm) of the telecommunication spectrum. These wavelengths are also popular for free-space optical communications; thus, our demonstrations are appropriately carried out using wavelengths near 1550 nm.

Figure 4 shows the predicted output angles of the directed beam for wavelengths from 1546 to 1590 nm using the equations shown previously and the parameters illustrated in Fig. 2. Here, we used a waveguide index, n_{awg} , of 1.5 and a ΔL of 199 μm to have the AWG operate in the 194th diffraction order at 1550 nm. We also assumed that there is no apodization from any apertures which might have limited the field. The figure shows 6 columns and 8 rows of achievable directions. Each row corresponds to a single channel from the AWG, and the horizontal separation between the rows is created by dispersion from the diffraction grating. The 6 columns are a result of fitting 5 FSRs ($\sim 8\text{nm}$ for the AWG) in the total wavelength range.

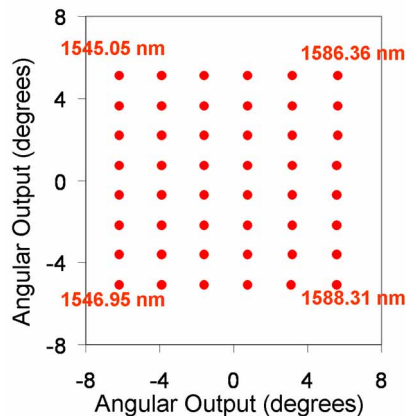


Fig. 4. Calculated output angles from the beam scanner.

Ideally, the range of a beam scanner should be continuous instead of a discrete array of spots. This functionality can be incorporated into our beam scanner with the addition of a continuous beam scanner to cover the range in between the spots. The requirements of this beam scanner are achievable with existing technology (such as an electro-optic scanner) since the required scanning range is now limited to the distance between our discrete directions.

4. Experimental results

Figure 5 shows a photograph of the actual setup where the output beam is projected onto a white screen 20 inches distant. We used a Sensors Unlimited 320M camera with visibility in the NIR wavelength range to image the projected beams. This photograph also shows an Agilent tunable laser as the optical source. In our experiments, we used a number of different optical sources to characterize different properties of the beam scanner. For fast beams scanning, the ideal source would be a fast, wavelength tunable laser. To the author's knowledge, the fastest tunable lasers are grating-assisted codirectional coupler with rear sampled reflector (GCSR) lasers which can switch across its entire wavelength range in under 50 ns⁹. The wavelengths from these lasers are limited to a discrete set of wavelengths; however, this does not harm our system's scanning ability.

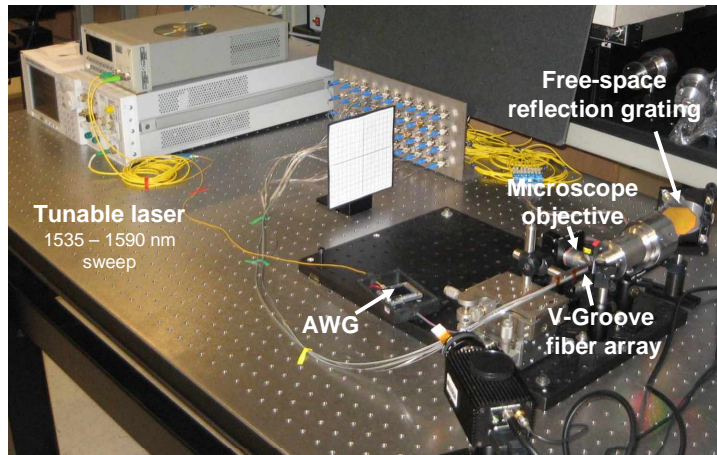


Fig. 5. Photograph of the beam scanner with a tunable laser acting as the optical source.

We used a C- and L-band ASE source to simultaneously transmit power into the entire output array of beams. Figure 6 shows the captured image of all of these beams projected onto the screen.

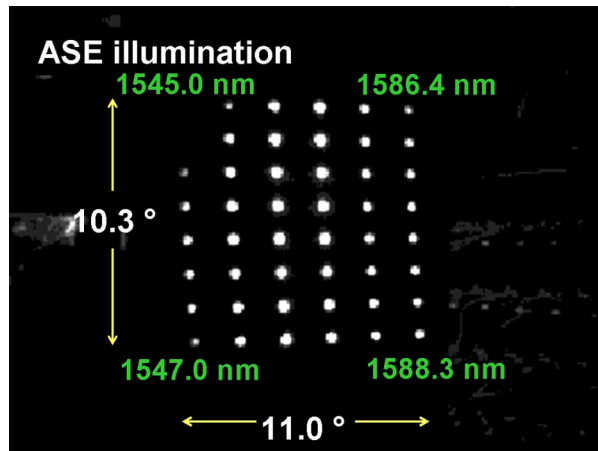


Fig. 6. An ASE optical source is used to send power towards every achievable direction of the beam scanner. The camera is saturated to show all spots.

Figure 6 shows that the achievable range from our beam scanner was 10.3° and 11.0° and exists as discrete directions in an 8 by 6 array. This is consistent with the predictions shown previously. The apparent power variation over the different directions is primarily due to the spectral profile of the ASE source. Previous work using these components as a wavelength demultiplexer instead of a beams scanner⁸ suggests that the insertion losses are uniform across the wavelength tuning range with approximately 8 dB loss.

For the next part of our experiments, we used an Agilent 81642A tunable laser to send power to a single direction. The output beam of a single wavelength is shown in Fig. 7(a). While this laser's slow tuning speed (2.8 seconds to scan through 100 nm) makes it infeasible for FSO beams scanning, the Agilent tunable laser was still useful in observing the output beam quality of the beam scanner. The beam profile is a result of a re-imaged fiber output (from the v-groove array) directed and collimated by the microscope objective. Figure 7(b) shows an image of the single spot. This was captured using a bare InGaAs sensor placed immediately after the output of the beam scanner. We measured a 6 mm $1/e^2$ beam diameter which

matches the expectations of a bare fiber output being collimated by the microscope objective. We note that this beam waist can be changed by selecting a different collimating lens.

Figure 7(b) also shows that the beam maintains a primarily Gaussian form which is indicative of low distortion through the system and yielding a smooth wavefront.

In previous work⁸, we showed that in these 2D dispersive systems, the crosstalk inherent in the AWG and the linewidth of the optical source determines the amount of crosstalk between neighboring wavelength channels. The prior results also show that there is virtually no (> 30 dB) crosstalk between channels which are separated by one FSR. Using the devices in our setup as an example, the Agilent laser linewidth is 100 kHz which is negligible compared to the 100 GHz AWG channel pitch. This means that the crosstalk is determined by the crosstalk between AWG channels which we measured as greater than 35 dB. Figure 7(a) also shows no apparent leakage of the optical power into neighboring channels.

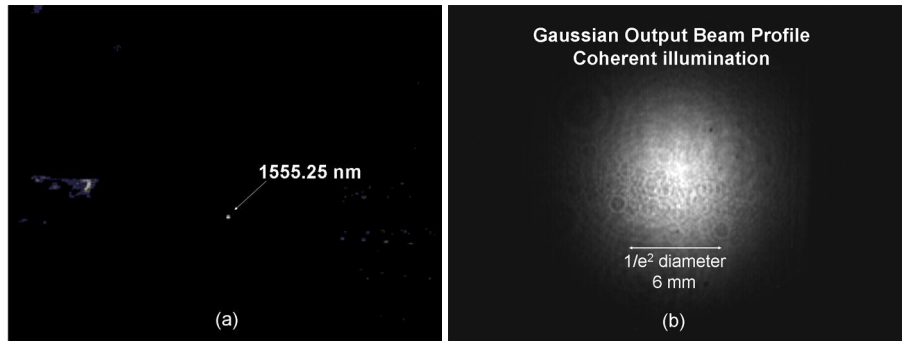


Fig. 7. (a). The output of a single wavelength and b) its profile immediately exiting the beamscanner.

Since this system is intended for use in FSO communications, the transmitted beam may carry a modulated signal and would inherit a finite bandwidth. Since our system is dispersive, a significant bandwidth would stretch the output beam over a linear range of directions. The amount of stretching would depend on the degree of dispersion of the free space optical grating. Crosstalk may also cause a limitation when the signal is modulated with a bandwidth greater than those of the AWG channels.

An alternative to using a tunable laser as the source is to use an ASE source passed through a tunable filter. We demonstrated this option using the same ASE source used above along with a CoreTek MEMS tunable etalon filter. Two separate detectors were placed at different points in the field of view. These points corresponded to 1546.7 nm and 1578.3 nm wavelengths. Figure 8 shows the transient response of the power at the simultaneously measured positions when the filter was switched between these two wavelengths. This shows a 183 μ s switching time which is purely determined by the switching speed of the tunable filter. The CoreTek MEMS filter used here had a passband of 0.47 nm which is larger than the channel pitch of our AWG. Thus, this filter produced approximately 5 dB of crosstalk in adjacent channels and would not be suitable as a secure FSO beamscanner.

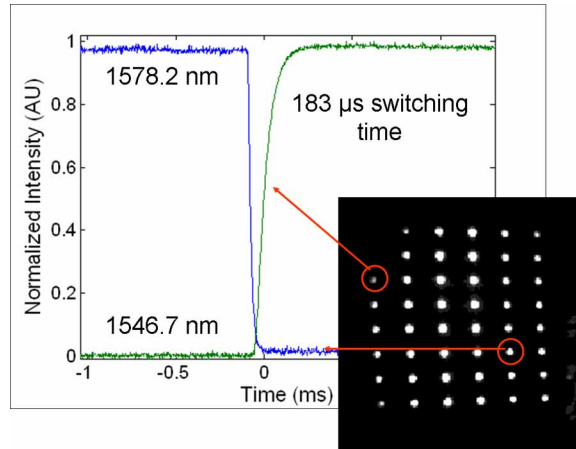


Fig. 8. Transient response when switching between two directions.

5. Beam scanner with VIPA

An alternative implementation of this beam scanner is one that uses a VIPA in place of the AWG. The VIPA, invented by M. Shirasaki¹⁰, is a glass slab that acts much like a highly dispersive diffraction grating. The VIPA operates on the principle of virtual images interfering with one another, as illustrated in Fig. 9. These virtual images are of a line source which is created by focusing a collimated beam with a cylindrical lens. This line source is focused at the entrance aperture of the glass slab which is tilted at a small angle. The back surface of the slab is nearly 100% reflective while the front slab has a graded reflectivity to allow output light. In this arrangement, the light will undergo multiple reflections and create a series of staggered virtual line sources. The light leaks out of the front surface into free-space where the cylindrical waves created by the virtual line sources interfere with each other. The graded reflectivity equalizes the leaked power of successive reflections. Ultimately, this resembles a diffraction grating operating with a large tilt and very high order.

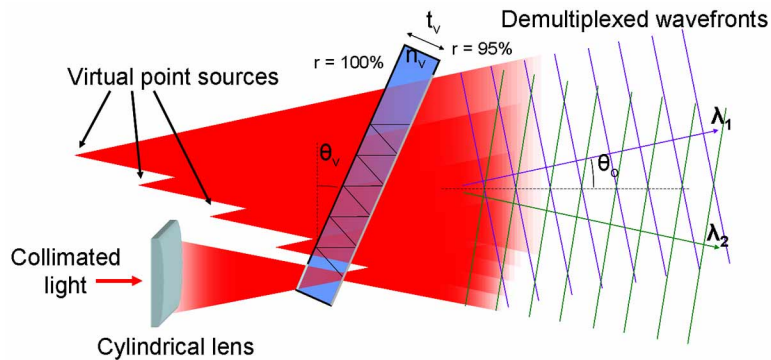


Fig. 9. A VIPA with the virtual line sources illustrated.

One beneficial advantage of the VIPA over the AWG is that the VIPA operates in a much higher diffraction order. This allows for more raster lines over a chosen wavelength range. This is described by the grating equation for the VIPA, Eq. (10), where m_v is the diffraction order, t_v is the thickness of the VIPA, n_v is its index of refraction, θ_v is the tilt angle of the VIPA and θ_o is the output angle.

$$\frac{m_v \lambda}{2t_v n_v} = \sin\left(\frac{\pi}{2} + \theta_o - \theta_v\right) \quad (10)$$

The output angle, θ_o is shown explicitly in Eq. (11).

$$\theta_o = \theta_v - \frac{\pi}{2} + \sin^{-1}\left(\frac{m_v \lambda}{2t_v n_v}\right) \quad (11)$$

The f-number of the cylindrical lens determines the field of view of the virtual line sources. This subsequently restricts the range of possible output angles, θ_o and will therefore keep the optical power in diffraction orders that fall within this angular range. In a beamscanner, especially one used for secure free-space optical communications, only one diffraction order should exist within the field of view for each wavelength. To ensure this, the optical path length of the VIPA, $t_v n_v$, inherits a maximum limit. When this optical path length is small, the value of the last factor in Eq. (11) is significantly different at adjacent diffraction orders. This difference should be large enough such that the adjacent diffraction orders fall outside the possible range of θ_o and only one diffraction order exists for each wavelength. This requirement is shown in Eq. 12 where $f_{\#}$ is the f-number of the cylindrical lens.

$$\tan^{-1}\left(\frac{2}{f_{\#}}\right) < \sin^{-1}\left(\frac{m_v \lambda}{2t_v n_v}\right) - \sin^{-1}\left(\frac{(m_v - 1)\lambda}{2t_v n_v}\right) \quad (12)$$

The VIPA is made into a 2D beamscanner by layering a diffraction grating on the VIPA's output surface. This is depicted in Fig. 10 where every wavelength, represented by different colors, is shown projecting out of the beamscanner. Also, a planar waveguide creates the line source entering the VIPA instead of a cylindrical lens. This creates a more seamless and compact integration of fiber optic input into the VIPA. The angular range of the cylindrical wave is now determined by diffraction from a slit. In other words, the angular range of the beamsteerer is inversely proportional to the width of the slit and independent of the total aperture. To increase the aperture size, the length of the line source can be mechanically increased and the transmissivity through exit surface of the VIPA can be decreased to create more internal reflections and distribute the power over a longer distance. Unlike the fiber coupled AWG, the VIPA gives a spatially continuous, free-space output meaning that the beamscanner can scan continuously along one of the directions.

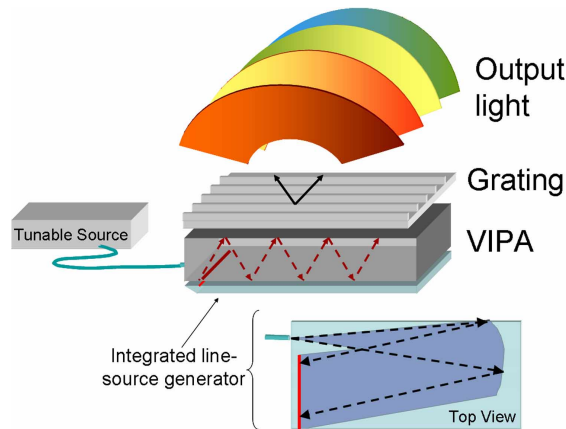


Fig. 10. Beam scanner consisting of a VIPA and a free-space optical grating demultiplexer.

Equation (10) can be used to find the wavelength range of each diffraction order in the VIPA's field of view as well as the output angle of each wavelength in one direction. The grating determines the output angle in the orthogonal direction which is predicted by Eq. (1).

We envisioned a VIPA beams scanning system with the following parameters to demonstrate its potential performance. The cylindrical wave feeding into the VIPA has a numerical aperture of 0.05 and the diffraction grating has a 500 lp/mm pitch operating in the 1st order. VIPAs typically have a 1.5 index, 1 mm thickness. Figure 11(a) shows the output if we use a typical VIPA tilted at 2.5° where the spots at 1553 nm are circled. This figure reveals that multiple diffraction orders are created. As mentioned earlier, this is because the optical path, $t_v n_v$, of the VIPA is too large.

In order to create a viable beams scanning system which transmits only one beam, the VIPA would have 1.5 index of refraction and 0.1 mm thickness. The thinness of the VIPA is atypical and may pose additional problems such as coupling the light into the slab, sturdiness or uniformity of the VIPA. For the purposes of this investigation, we assumed that such a device could exist and operate with the same properties of a typical VIPA. The same section of the output is shown in Fig. 11(b) with the thinner VIPA.

Figure 12 shows the entire calculated output field where the optical wavelength range used is 1400 – 1600 nm. With these parameters, Fig. 12 shows approximately 5° x 9° total output range existing over 26 columns of output angles.

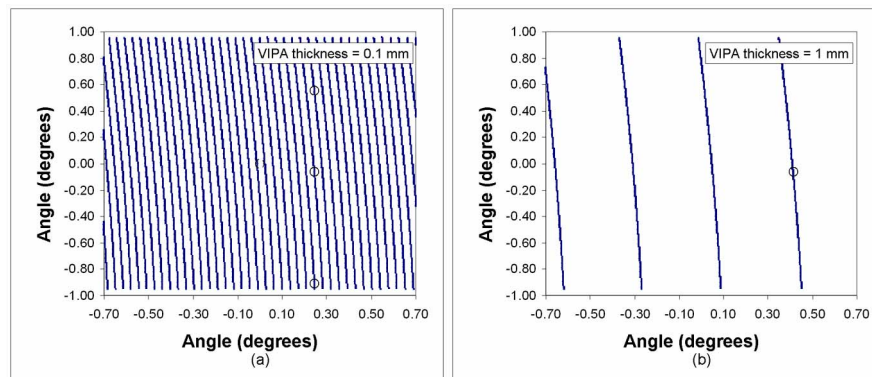


Fig. 11. A section of the output of a 2D demultiplexer which uses a) a 1 mm thick VIPA and b) a 0.1 mm thick VIPA. Spots created at 1553 nm are circled and show degeneracy through multiple diffraction orders when the VIPA is too thick. For secure FSO communications, only one diffraction order should exist.

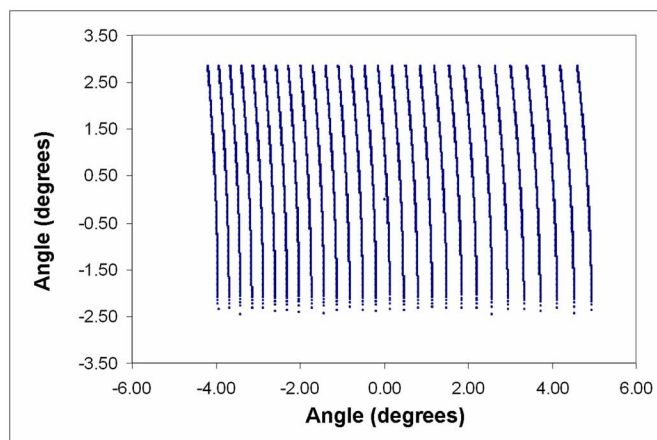


Fig. 12. Calculated output directions (in degrees) using a VIPA in the beam scanner.

6. Conclusion and discussion

We presented a beamscanning method where the input wavelength is directly related to the output direction in a 2-dimensional field of view. This is accomplished by combining two wavelength dispersive devices orthogonally and in series. With the proper devices, the beam raster scans through the 2-dimensional field as the wavelength from an optical source is increased.

We have experimentally demonstrated beamscanning by combining an AWG with a free-space optical grating demultiplexer. Using this combination of parts, we obtained 2-dimensional beamscanning on an 8x6 grid of discrete directions. This output was directed using a 25 mm focal length microscope objective resulting in a total angular range of 10.3° by 11.0°. These results were consistent with calculations based on diffractive theory and geometric optics. We achieved 183 μ s scanning times using an ASE source followed by a CoreTek tunable filter which switched the power from 1546.7 nm to 1578.2 nm.

We also discussed an improved version of the beam scanner which uses a VIPA combined with a free-space optical grating demultiplexer. Because the VIPA has a continuous output, one dimension in the output field of view can be scanned continuously. In the other dimension, the high dispersion of the VIPA allows us to point to a greater number of discrete directions which are spaced closer together. This was verified with theoretical calculations on a conceptual system.

Acknowledgments

The authors would like to acknowledge DARPA Systems Microsystems Technology Office for their support in this work.